RMetS
Royal Meteorological Society

The role of boundary-layer friction on tropical cyclogenesis and subsequent intensification

Gerard Kilroy,[a]* Michael T. Montgomery[b] and Roger K. Smith[a]
[a]*Meteorological Institute, Ludwig Maximilians University of Munich, Germany*
[b]*Department of Meteorology, Naval Postgraduate School, Monterey, CA, USA*

*Correspondence to: G. Kilroy, Meteorological Institute, Ludwig-Maximilians University of Munich, Theresienstrasse 37, 80333 Munich, Germany. E-mail: gerard.kilroy@lmu.de

A recent idealized, high-resolution, numerical model simulation of tropical cyclogenesis is compared with a simulation in which the surface drag is set to zero. It is shown that, while spin-up occurs in both simulations, the vortex in the one without surface drag takes over twice as long to reach its intensification begin time. When surface friction is not included, the inner core size of the simulated vortex is considerably larger and the subsequent vortex intensity is significantly weaker than in the case with friction. In the absence of surface drag, the convection eventually develops without any systematic organization and lies often outside the radius of azimuthally averaged maximum tangential winds. The results underscore the crucial role of friction in organizing deep convection in the inner core of the nascent vortex and raise the possibility that the timing of tropical cyclogenesis in numerical models may have an important dependence on the boundary-layer parametrization scheme used in the model.

Key Words: tropical cyclone; hurricane; typhoon; spin-up; cyclogenesis; intensification

Received 3 February 2017; Revised 18 May 2017; Accepted 19 June 2017; Published online in Wiley Online Library

1. Introduction

The importance of the boundary layer in tropical cyclone behaviour has been recognized for many decades (Charney and Eliassen, 1964; Ooyama, 1969; Rosenthal, 1971; Anthes, 1974; Emanuel, 1986, 1997; and references therein). For a long time its role was seen as feeding moisture inwards to maintain the inner-core deep convection, much of the moisture being picked up at the ocean surface through evaporation. Gradually its dynamical role in the spinning up of the low-level winds, as well as the winds in the developing eyewall region, was recognized (Carrier, 1971; Anthes, 1974; Smith *et al.*, 2009; Schmidt and Smith, 2016).

Because of the high Reynolds numbers of atmospheric vortices, the frictional boundary layer is generally turbulent. Traditionally, the corresponding vertical turbulent momentum flux near the surface is modelled in terms of a bulk aerodynamic formula equal to the product of a drag coefficient C_D and the square of the near-surface wind speed. Likewise, the turbulent enthalpy flux from the sea surface is modelled also using a bulk aerodynamic formula that equals the product of an enthalpy exchange coefficient C_K, the near-surface wind speed and the air–sea disequilibrium of enthalpy.

A number of studies have investigated the effects of the boundary layer in a full cyclone model by varying the turbulent exchange coefficients of momentum and enthalpy. The early experiments of this type were based on axisymmetric numerical models, using either parametrized convection (Ooyama, 1969; Rosenthal, 1971; Emanuel, 1989, 1995), or relatively coarse, convection-permitting, configurations (Craig and Gray, 1996). Later studies employed higher-resolution axisymmetric representations of moist convection phenomenology (Bryan and Rotunno, 2009) and three-dimensional convection-permitting configurations (Montgomery *et al.*, 2010; Schecter, 2011; Bryan, 2012; Persing *et al.*, 2013; Smith *et al.*, 2014).

1.1. Dependence of vortex intensification on surface drag

In one of the earliest studies Rosenthal (1971), used an axisymmetric, multi-level, primitive equation model with a modified Kuo cumulus parametrization scheme to examine the dependence of the intensification rate on the drag coefficient. At that time, following Charney and Eliassen (1964), the prevailing idea was that surface drag played a dual role in the tropical cyclone development. In the boundary layer, the reduction of the tangential wind due to surface friction results in an imbalance of forces in the radial direction and leads to inflowing air which, as noted above, supplies the inner-core clouds with moisture through the evaporation of water from the underlying ocean. On the other hand, a higher surface drag leads to a higher frictional torque on the tangential wind.

From an energetics perspective, the quadratic nature of the frictional drag law implies a cubic dependence of the kinetic energy dissipation rate on wind speed in the boundary layer. Since the energy input to the system is controlled largely by the moist enthalpy fluxes, which are proportional to near-surface wind speed to leading order, the frictional dissipation ultimately dominates and arrests the intensification process. These ideas were already evident in some of Ooyama's (1969) experiments where it was shown that the mature final intensity of the model cyclone decreases as the drag coefficient increases. These ideas

were corroborated by Rosenthal (1971) who, in reference to his figure 9, noted that 'decreased drag coefficients ... lead to smaller growth rates but greater peak intensities'. Rosenthal noted also that one should expect no growth at all when C_D is decreased to zero. However, Rosenthal's conclusions on this latter point need to be considered with caution, because they are dependent upon the assumed Kuo cumulus parametrization which links the convective mass flux with the frictional convergence in the boundary layer.

In a later study using an axisymmetric convection-permitting model, Craig and Gray (1996) found that the rate of intensification increases with increasing values of the transfer coefficients for heat and moisture. They found also that the intensification rate is relatively insensitive to changes in the drag coefficient and noted that 'frictional convergence is of secondary importance [for intensification], but may represent a sink of energy that decreases the growth rate'. An interesting result of Craig and Gray's study was the finding that the largest intensification rate was obtained with no surface friction at all (their p. 3537), a result that is opposite to that of Rosenthal.

Montgomery *et al.* (2010) used a three-dimensional, convection-permitting model to investigate the sensitivity of the intensification rate to the model drag coefficient. They presented a series of experiments in which the intensification rate and intensity of the vortex were found to increase with increasing surface drag coefficient until a certain threshold value was attained and then the intensification rate and intensity decreased. When the drag coefficient was set to zero, no system-scale intensification occurred on a time-scale of 4 days, despite persistent sea-to-air fluxes of moisture that maintain deep convective activity. In a follow-up study, Smith *et al.* (2014) extended these calculations to include a wind-speed-dependent drag coefficient and one of four boundary-layer parametrization schemes. On realistic forecast time-scales (5 days), they found that the changes in vortex behaviour with changing drag coefficient were qualitatively similar among all schemes. The maximum intensification occurred for a value somewhere near the standard value of the drag coefficient.

1.2. *A resolution of different model results*

A resolution of the discrepancy in the dependence of the vortex intensification rate found by Craig and Gray (1996) compared with that found by Montgomery *et al.* (2010) and Smith *et al.* (2014) was provided by Persing *et al.* (2013), who highlighted *inter alia* the intrinsic differences in the behaviour of deep convection in axisymmetric and three-dimensional vortices (their figure 21). On a time-scale of 12 days, the three-dimensional simulation with the lowest drag struggled to develop, while that in the axisymmetric simulation developed relatively rapidly and the intensity after 8 days became unrealistically large. The reason for the more rapid growth in the axisymmetic configuration was found to be linked to the much larger diabatic heating rate and associated radial gradient thereof in the axisymmetric calculation. This result is related to the organization of deep convection in the two model configurations, the convection in the axisymmetric model being already organized into convective rings. In the three-dimensional model, such geometric organization of the convection cannot be assumed at early times and the frictional convergence aids the organization process.

Schecter (2011) examined the consequences of setting the surface drag to zero for tropical cyclone formation and intensification. Although focused primarily on the evaluation of a reduced model based on Ooyama's (1969) classical three-layer formulation, generalized to three dimensions and including a number of convective parametrization schemes*, Schecter conducted high-resolution, three-dimensional, near-cloud-resolving experiments using the Regional Atmospheric Modeling System (RAMS; Cotton *et al.*, 2001, and references) to gauge the performance of the reduced model. Pertinent to the foregoing discussion were noteworthy experiments conducted with the RAMS model in which the surface drag coefficient was set to zero during the early organization phase of an emergent vortex. In these experiments, the exchange coefficients for latent and sensible heat transfer for a 'cool' ocean (SST = 26 °C) were unaltered from their standard control values. Schecter (his section 2.2) found that 'Initially, eliminating surface drag has little effect on the acceleration of wind speed. However, removing the influence of surface drag on boundary-layer convergence and convective organization ultimately inhibits hurricane formation'. With zero surface drag, he found that there was no sign of hurricane formation during a 30 day simulation. Consistent with Persing *et al.* (2013), Schecter (his section 2.2) noted a subtle influence of surface drag in the RAMS experiments: 'The influence of surface drag remains minimal 7.33 days into genesis, but seems to nudge convection toward the centre of the developing domain-scale circulation'. We will return to comment on this insightful finding in Section 8.

1.3. *The rotating convection paradigm for vortex intensification*

Recent work has proposed a new overarching framework for understanding the intensification and structure change of tropical cyclones. This framework, which has been referred to as the rotating convection paradigm for tropical cyclone intensification, recognizes the role of rotating deep convective clouds and their aggregate effects on driving a system-scale overturning circulation. In turn, this circulation acts to concentrate absolute vorticity in the lower troposphere, some of the vorticity amplified by prior deep convection, and thereby, through Stokes' theorem, to increase the circulation about fixed circuits in and around the convective region. A recent review of the process from both an aggregate and eddy-resolving perspective is given by Montgomery and Smith (2017) and in an abridged version by Smith and Montgomery (2016a).

An important aspect of the rotating convection paradigm is the role of the frictional boundary layer, in which, as the vortex intensifies, the spin-up of the maximum tangential wind speed occurs. This feature, which may seem counter-intuitive, was already anticipated by Anthes (1974, p. 506). It has since been found in observational analyses and was identified by Smith *et al.* (2009) as an important element of the spin-up process. Smith *et al.* (2009) referred to this element as *the boundary-layer spin-up mechanism* to distinguish it from the classical spin-up mechanism, which was articulated by Ooyama (1969, 1982) and involves the concentration of absolute vorticity above the boundary layer by the convectively driven secondary circulation referred to above.

The rotating convection paradigm has been invoked in recent work to explain the dependence of intensification rate on latitude (Smith *et al.*, 2015a) and sea surface temperature (Črnivec *et al.*, 2016). It has been used also to explain how the boundary layer exerts a progressive control on the inner core expansion as the vortex matures (Kilroy *et al.*, 2016a), and to explain the spin-up of the eyewall cloud region (Persing *et al.*, 2013; Schmidt and Smith, 2016).

1.4. *A unified theory of genesis and intensification*

In another recent paper, the rotating convection paradigm has been shown to extend to understanding tropical cyclogenesis in a favourable environment (Kilroy *et al.*, 2017, hereafter KSM). The paper describes a three-dimensional, near-cloud-resolving (horizontal grid spacing 500 m), warm rain† simulation of genesis in a quiescent environment, starting from a weak cyclonic

*This reduced model was used also as the basis for a related study of diabatic Ekman turbulence (Schecter and Dunkerton, 2009).

†An extension of the study to examine the effects of ice microphysics is currently underway.

vortex (maximum wind speed 5 m s^{-1}) in thermal-wind balance. Evidence was presented in their section 4 that the boundary layer begins to exert an important influence on the inner-core flow by the time that significant intensification begins. Even at this stage, the maximum azimuthally averaged wind speed is no more than approximately 10 m s^{-1}. The importance of the boundary layer at early times was already indicated in calculations by Montgomery *et al.* (2006), who noted that surface drag accelerates the genesis process and contributes to the strong contraction of the vortex as the vortex develops (their Table and Experiment D2). These authors did not further investigate the role of surface friction in the genesis process.

1.5. The present study

The purpose of the present paper is to further investigate the subtle role of frictional effects in the genesis process. We do this by comparing the control calculation of KSM with one in which the drag coefficient is set to zero. The remaining paper is organized as follows. Section 2 describes the model configuration and the two numerical simulations carried out. Section 3 presents diagnostic analyses of the two simulations, while section 4 investigates the early differences in convective evolution in both experiments. Section 5 investigates the importance of boundary-layer dynamics at early times. Section 6 provides an explanation for vortex spin-up in the simulation without friction. Section 7 presents an azimuthally averaged view of vortex evolution in both simulations, while section 8 compares our findings with those of previous work on the topic. The conclusions are given in section 9.

2. The numerical model and experimental design

This study focuses on two high-resolution three-dimensional simulations, the control experiment in KSM and a rerun of this simulation with surface drag switched off.

The simulation with surface drag switched off has the same basic configuration as described in KSM. It relates to the evolution of a prescribed, initially weak, cloud-free, axisymmetric vortex in a quiescent environment on an f-plane and uses the numerical model CM1 version 16, a non-hydrostatic and fully compressible cloud model (Bryan and Fritsch, 2002). In brief, the outer domain is 3000 × 3000 km in size with variable horizontal grid spacing reaching 10 km near the domain boundaries. The inner domain is 300 × 300 km in size and has a uniform horizontal grid spacing of 500 m. The domain has 40 vertical levels extending to a height of 25 km. The vertical grid spacing expands gradually from 50 m near the surface to 1200 m at the top of the domain. The simulation is carried out on an f-plane with the Coriolis parameter $f = 2.53 \times 10^{-5}$ s^{-1}, corresponding to 10°N. The balanced initial vortex has a maximum tangential wind speed of 5 m s^{-1} at the surface at a radius of 100 km. Surface enthalpy fluxes are present in both simulations. The subgrid turbulence scheme used is the model option *iturb=3*, a parametrized turbulence scheme with no explicit turbulence (Bryan and Rotunno, 2009). A simple warm-rain scheme is used in which rain has a fixed fall speed of 7 m s^{-1}. As in KSM, radiative effects are represented by adopting a Newtonian cooling approximation capped at 2 K day^{-1}, following Rotunno and Emanuel (1987). The only differences in the model set-up from that in KSM are that the surface drag is switched off (i.e. *idrag=0*), a zero-gradient boundary condition is chosen[‡] (i.e. *bcturbu=2*) and the simulation is integrated for a longer period of time (240 h instead of 108 h) because of the longer time required for the vortex to intensify.

In order to reduce the amount of output data produced for the no-friction control experiment, the data are stored at 15 min intervals before 108 h and every 3 h beyond this time.

The reference sounding is described in KSM (their figure 1). In brief, it is a mean of 39 dropsonde soundings obtained on 12 September 2010, during the PREDICT (PRE-Depression Investigation of Cloud systems in the Tropics) field campaign for the tropical wave-pouch disturbance that eventually became tropical storm *Karl* late in the afternoon of 14 September (local time) (Montgomery *et al.*, 2012; Smith and Montgomery, 2012 give details). This mean sounding has a Convective Available Potential Energy (CAPE)[§] of 2028 J kg^{-1}, a Convective Inhibition (CIN)[¶] of 47 J kg^{-1} and a Total Precipitable Water (TPW) value of 61 kg m^{-2}. The sea surface temperature (SST) is 29°C, typical of the Caribbean region at the time.

3. Vortex evolution with and without friction

In the descriptions that follow, we refer to the zero drag simulation as Ex-NoFr and the control experiment from KSM that includes surface drag as Ex-Fr. Figure 1 compares the evolution of certain metrics characterizing the azimuthally averaged behaviour of these two simulations, including the maximum tangential wind speed (V_{max}), the radius at which this maximum occurs (R_{vmax}) and the temporally smoothed (1-2-1 filter, used five times) maximum vertical velocity (W_{max}). Also shown is the maximum local total horizontal wind speed, VT_{max}.

The V_{max} curves for both simulations remain almost identical until about 36 h. After this time the curves begin to diverge and at 45 h, the vortex in Ex-Fr begins a rapid intensification (RI)[‖] phase. This time is referred to as the intensification begin time in KSM. During the following 36 h, V_{max} in Ex-Fr increases from about 10 m s^{-1} to about 70 m s^{-1}. In Ex-NoFr, V_{max} increases by only 10 m s^{-1} during the first 108 h. It increases less rapidly than in Ex-Fr to nearly 50 m s^{-1} over the next 60 h and after 168 h it starts to decline. In both experiments, VT_{max} is larger than the corresponding azimuthally averaged V_{max} at all times, a consequence of velocity fluctuations associated with deep convection.

In both simulations, R_{vmax} begins to fluctuate as soon as deep convection begins to develop. In Ex-Fr, R_{vmax} decreases gradually until about 48 h and then falls rapidly to a value of about 10 km. Thereafter, its value does not change appreciably over the next 60 h. In Ex-NoFr, R_{vmax} fluctuates wildly throughout the first 120 h of the integration, although there is a downward trend, indicating that some deep convection occurs within the radius of maximum winds. Between 130 and 170 h, R_{vmax} settles on a value of around 35 km, after which it gradually increases to about 50 km at 240 h.

In Ex-Fr, W_{max} starts to increase at about 12 h when the first bout of deep convection occurs. It reaches a small peak about 6 h later and then declines to near zero at around 24 h. Thereafter, it begins a gradual increase over the next 48 h as the convection focuses near the centre of the circulation.

In Ex-NoFr, W_{max} remains relatively small in comparison to that in Ex-Fr until 108 h (0.5 m s^{-1} or less up to this time) when it gradually increases to attain a lifetime maximum of not quite 1.5 m s^{-1} at about 144 h. Thereafter, it steadily declines. The

[‡]There appears to be a non-zero turbulent stress calculated even when the model option *idrag=0* is chosen, leading to a reduction in the near-surface winds from the initial time. To circumvent this issue, a zero-gradient lower boundary condition must be chosen also.

[§]We remind the reader that CAPE is a parcel quantity that typically has a strong negative vertical gradient in the lower troposphere. For this reason, the values cited herein are based on an average for air parcels lifted from the surface and at 100 m intervals above the surface to a height of 500 m. Since the calculation of CAPE is a nonlinear function of temperature and moisture, we prefer this method to one based on averaged values of temperature and mixing ratio through a surface-based layer of air with some arbitrarily prescribed depth.

[¶]Like CAPE, CIN is a quantity that refers also to an air parcel. Rather than computing an average up to 500 m as for CAPE, it seems physically more reasonable to examine the minimum value of CIN up to this level.

[‖]In the tropical cyclone community, RI is typically defined as an increase in the near-surface total wind speed exceeding about 15 m s^{-1} over a period of 24 h (Kaplan and DeMaria, 2003).

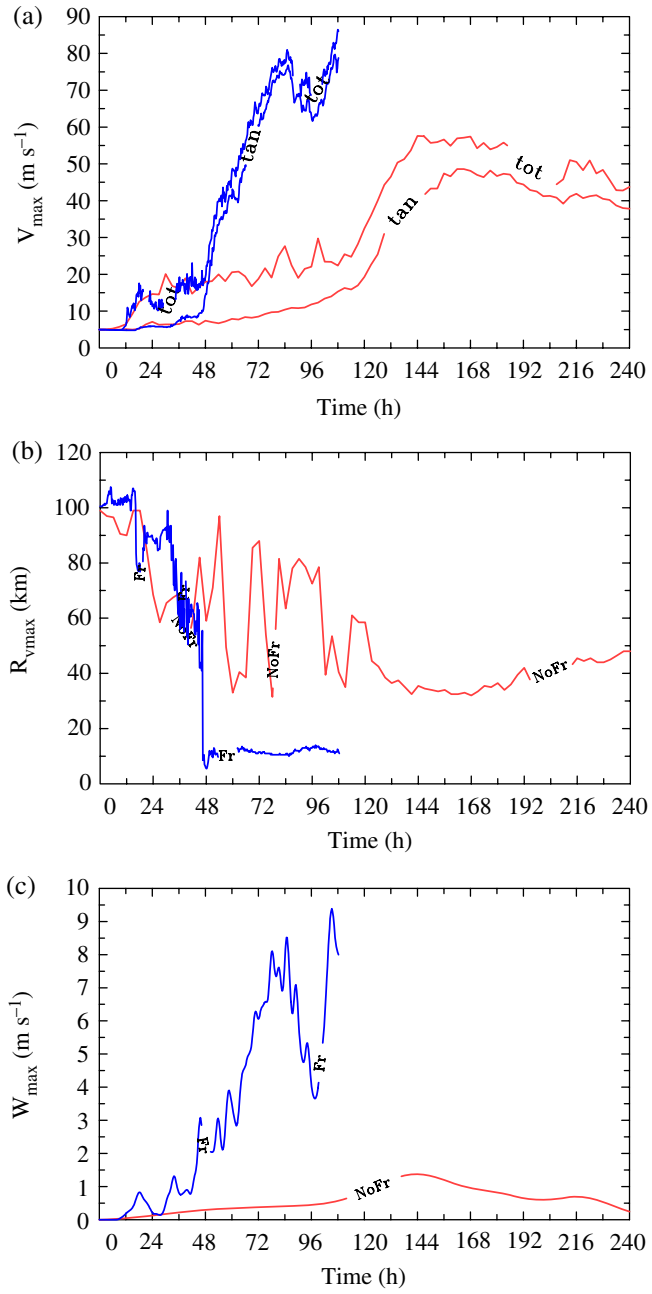

Figure 1. Time series of (a) maximum total wind speed (VT_{max}, tot) and maximum azimuthally averaged tangential wind speed (V_{max}, tan), (b) the radius R_{vmax} at which the maximum tangential wind speed (V_{max}) occurs, and (c) the azimuthally averaged maximum vertical velocity (W_{max}). Blue curves are for Ex-Fr, red curves are for Ex-NoFr. [Colour figure can be viewed at wileyonlinelibrary.com].

comparatively small values of W_{max} in Ex-NoFr suggest that either the deep convective updraughts are much weaker than in Ex-Fr, or that deep convection that does form is located at relatively large radii and does not occupy an appreciable range of azimuth. The first possibility can be dismissed by a time series of the maximum total vertical velocity (at any given height or location), indicating that the strongest convection is typically the same magnitude in both experiments (not shown). This result suggests that deep convection occurs at larger radii in Ex-NoFr than in Ex-Fr. The suggestion is confirmed by an inspection of horizontal cross-sections of vertical velocity in the middle troposphere and is implicit also in the height–time series of vertical mass flux shown in Figure 2. These results underscore the crucial role of friction in organizing deep convection in the inner core of the nascent vortex.

Recently, the occurrence of deep convection close to the centre of an existing circulation has been highlighted as an important feature in the development of incipient tropical disturbances into cyclones (e.g. Smith *et al.*, 2015b; Tang *et al.*, 2016; Kilroy *et al.*, 2016b). This preferred location is not, as frequently supposed, because deep convection is more 'efficient' in this location on account of the higher inertial stability there (Smith and Montgomery, 2016b). Rather, the centre of an incipient vortex (or wave-pouch) takes on a preferential role because the convectively induced inflow is then able to draw in the absolute angular momentum (or M-)surfaces above the frictional boundary layer to small radii (e.g. Smith and Montgomery, 2016b, section 3.2). Irrespective of whether M is materially conserved, any inward movement of the M-surfaces implies a spin-up of the tangential winds.

Figure 2 shows the structure of vertical mass flux averaged over vertical columns with square cross-sectional areas 20 km × 20 km and 60 km × 60 km centred on the vortex centre** as a function of height and time in Ex-Fr and Ex-NoFr. There are striking differences between the time evolution of the mass flux in the two simulations in both sizes of column. While there are sporadic periods of upward mass flux in Ex-NoFr in both sizes of column, the bursts of deep convection that are characterized by these periods are not sustained, at least out to 48 h. In contrast, in Ex-Fr there is a 6 h period of marked convective activity between about 18 h and 24 h followed by a 6 h period of suppressed convection. After this suppressed period, deep convection develops strongly and persists in both columns. The persistence of convection in the innermost column, in particular, represents favourable conditions for vortex development and, indeed, in Ex-Fr, the vortex begins its RI phase after 45 h (Figure 1(a)).

Three pertinent questions arise at this point:
(i) what are the essential differences in convective behaviour between the friction and no-friction simulations?;
(ii) how does friction support the local convective organization and rapid intensification?; and
(iii) how does the vortex spin up in the no-friction experiment?
The next three sections are devoted to answering these questions.

4. Interpretation of differences in convective behaviour

On the basis of simple parcel theory, in order for deep convection to occur near the circulation centre, there must be both low CIN and adequate CAPE there. As we will show, the frictionally induced inflow associated with boundary-layer dynamics plays a fundamental role in providing these conditions, which, in turn, provide for vortex spin-up on a realistic time-scale of a few days.

Figure 3 shows the evolution of CAPE and CIN for both simulations until 120 h. Like Figures 2(a) and (c), the inner-core quantities are defined here as averages across a 20 × 20 km column centred on the circulation centre. In Ex-Fr there is a build-up of CAPE until about 30 h, after which time there is a sharp reduction over the following 5 h. This sharp reduction in CAPE is due to a burst of deep convection in the 20 × 20 km column at this time (as confirmed by animations of the fields, not shown). The CIN reduces to half its initial value by 24 h, followed by a small increase and then a precipitous fall to near zero a little after 36 h. RI occurs about 12 h later.

In Ex-NoFr there is no initial build-up of CAPE. There is a small reduction of CAPE at about 45 h, but the CIN is larger than its initial value until about 100 h. After 100 h the CIN reduces slightly (to about 20 J kg^{-1}), but at no point in the first 120 h shown here does the CIN become close to zero. A key question then arises: why is the CIN so large in Ex-NoFr?

To answer this question we show in Figure 4 azimuthally averaged Hovmöller plots of the water vapour mixing ratio difference (Δq) from that at the initial time for both experiments

**As in KSM, the vortex centre is found by searching for the surface pressure minimum in a filtered pressure field, with a requirement that the vortex is not allowed to move more than 20 km in a single time step. This prevents the centre-finding algorithm from locking on to a localized region of strong convection.

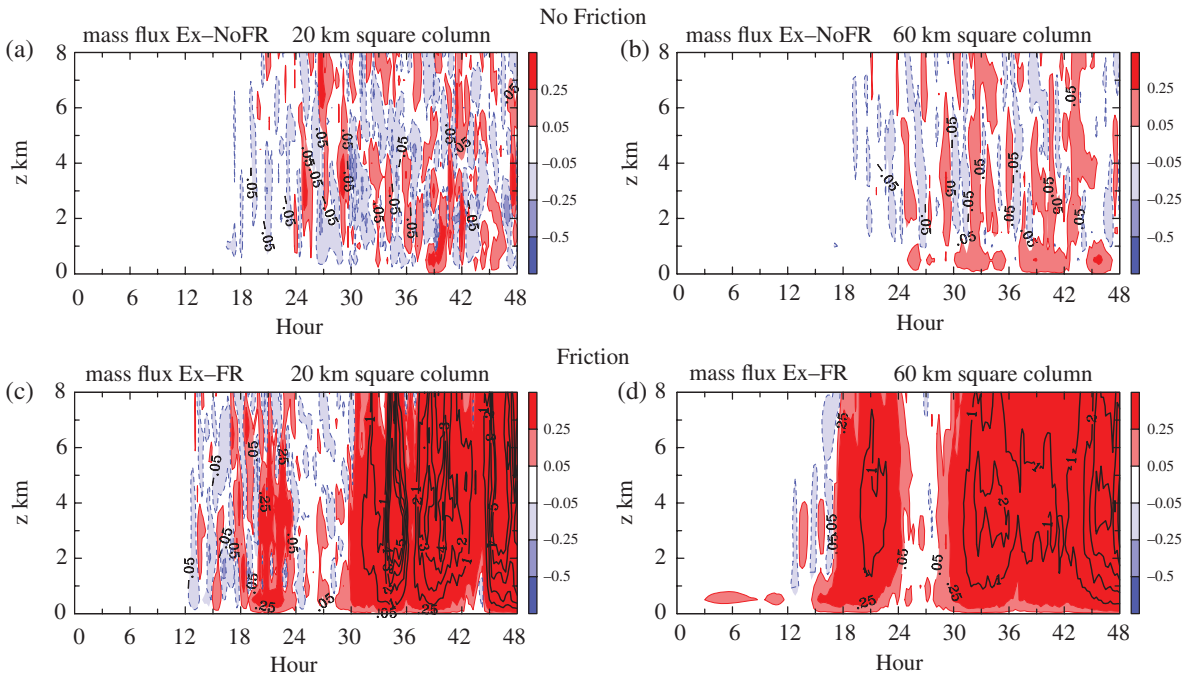

Figure 2. Time–height cross-sections of system-averaged mass flux within (a, c) a 20 km × 20 km column and (b, d) a 60 km × 60 km column, centred on the circulation centre. (a, b) show Ex-NoFr, and (c, d) Ex-FR. Values for the shading of mass flux are given in the colour bar, in units kg m^{-2}s^{-1}, multiplied by 10 for plotting purposes. Thick black contours are for values above 0.1 kg m^{-2}s^{-1}, at 0.1 kg m^{-2}s^{-1} intervals. [Colour figure can be viewed at wileyonlinelibrary.com].

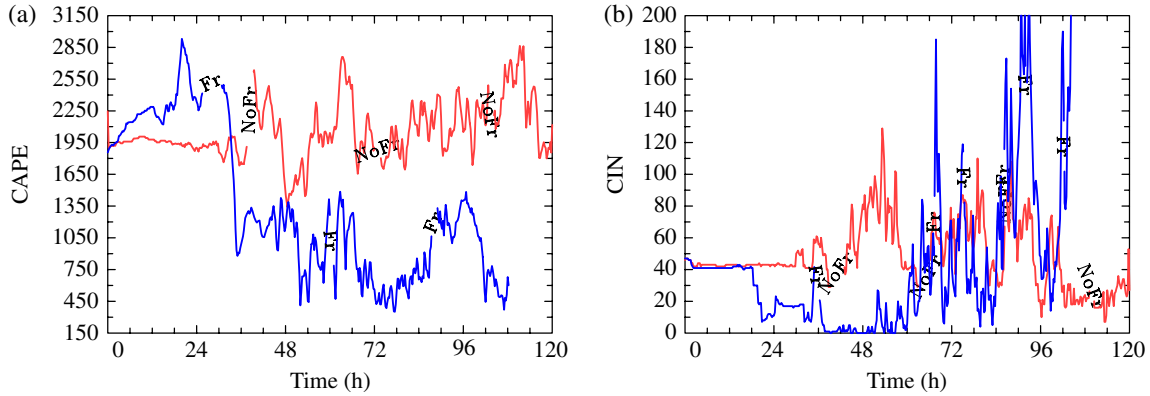

Figure 3. Evolution of (a) CAPE and (b) CIN, calculated from a sounding of an inner core average 20 km × 20 km column out to 120 h in the two experiments Ex-FR (FR) and Ex-NoFR (NoFr). [Colour figure can be viewed at wileyonlinelibrary.com].

at heights of 1 and 3 km out to 48 h. As early as 4 h there is moistening in Ex-Fr at a height of 1 km. This increase is a result of the lifting of boundary-layer air produced by the frictional convergence that begins at the initial time when surface drag is imposed (section 5). At 10 h the effects of convection are evident at radii between 45 and 60 km, as evidenced by an increase in moisture (0.5 g kg^{-1}) at this time. At 12 h the effects of convective moistening are seen at a radius of 60 km at a height of 3 km also. There is a continual moistening at smaller radii, during the 48 h period shown.

In contrast, in Ex-NoFr, there is no moistening at early times as in Ex-Fr. In fact, the first notable Δq at a height of 1 km appears at about 15 h. At this time drying is evident to a radius of 55 km, but beyond, at least to 100 km, there is a moistening. Subsequently, there is a progressive moistening as deep convection gradually migrates inwards to smaller radii. Even as the dry region decreases in size, the strongest drying ($\Delta q < -1$ g kg^{-1}) occurs inside a radius of 25 km from 42 h (thick black dashed contour). This drying must be associated with weak subsidence induced by deep convection at larger radii. A major difference in the two experiments is that, in Ex-NoFr, there is no mechanism to focus deep convection close to the circulation centre. As shown in the next section, boundary-layer dynamics in Ex-Fr play an important role in focusing the convection inside the radius of maximum tangential winds, thereby increasing the moisture in that region.

5. The role of the boundary layer

Kilroy *et al.* (2016a) employed a simple, steady, slab boundary-layer model to help explain the radial expansion of the inner core of a mature tropical cyclone. They showed that, when forced by the radially expanding azimuthally averaged tangential wind field at the top of the boundary layer from the numerical model simulation, the slab boundary-layer model correctly predicts the radial expansion of the radial and tangential velocity components in the inner core boundary layer, as well as the vertical velocity at the top of the boundary layer.

To investigate the role of the boundary layer in the genesis process, we employ the same slab boundary-layer model as Kilroy *et al.* (2016a). The details of this model and the justification for its use are given in Smith *et al.* (2015). We assume that the boundary layer has a uniform depth of 1000 m.

Figure 5 shows solutions for the radial, tangential and vertical wind components, u_b, v_b and w_b, for the steady, slab boundary layer with the gradient wind profile used to initialize the calculations (this profile has a maximum tangential wind speed of 5 m s^{-1} at a radius of 100 km). Because the initial vortex is relatively weak, the tangential wind in the boundary layer is essentially the same as that above the boundary layer at all radii, indicating that a linear approximation for the boundary layer may be appropriate. Indeed, it is found that the linear solution

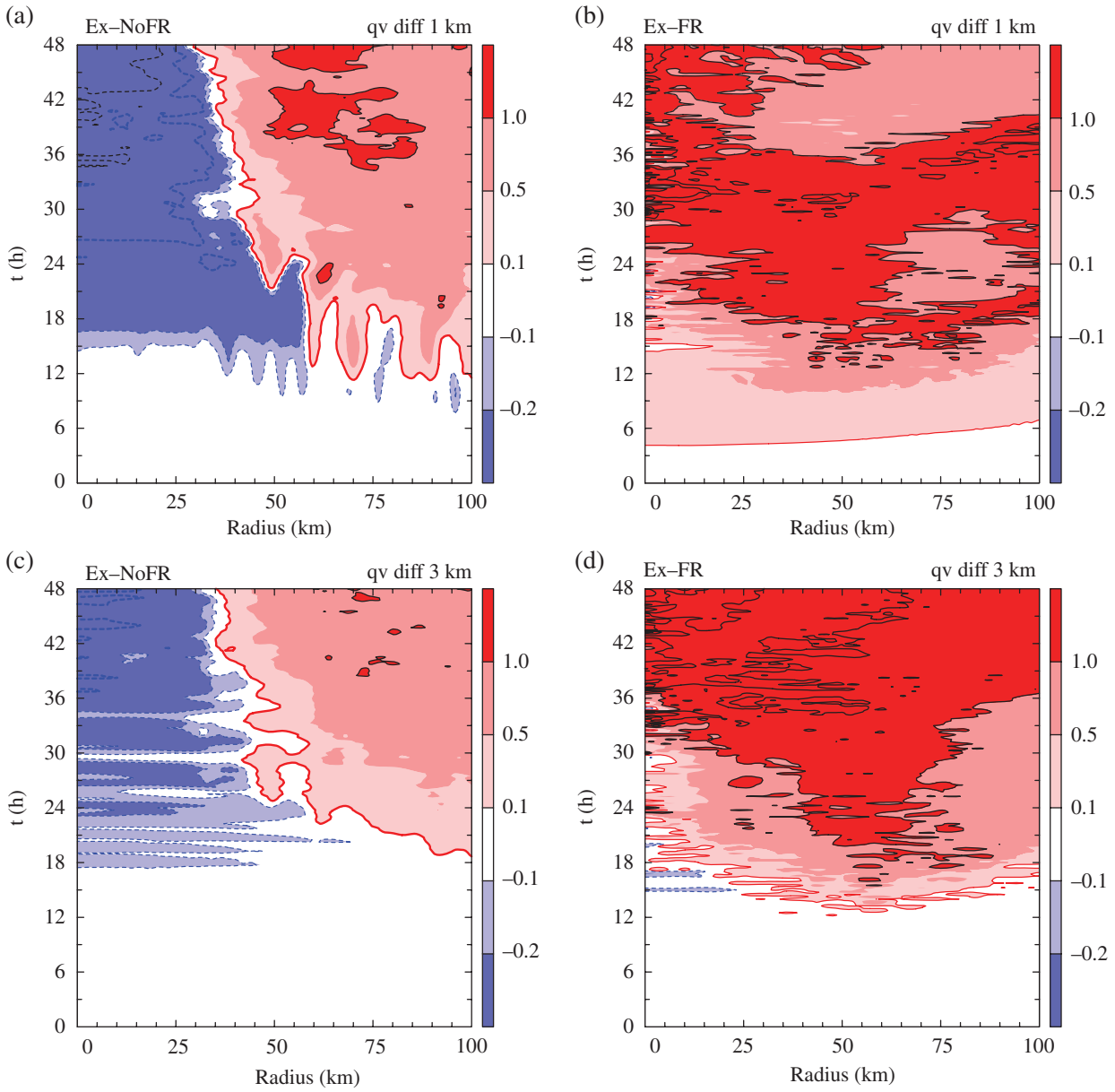

Figure 4. Azimuthally averaged Hovmöller plot of water vapour mixing ratio difference (shading, g kg^{-1}) from the initial profile at a height of (a, b) 1 km and (c, d) 3 km for (a, c) Ex-NoFr and (b, d) Ex-FR out to a radius of 100 km for the first 48 h of the simulation. The bold contours are −0.5 g kg^{-1} (blue dashed) and −1.0 g kg^{-1} (black solid). [Colour figure can be viewed at wileyonlinelibrary.com].

for the radial wind component is virtually coincident with the nonlinear solution (Figure 5(a)). The vertical velocity at the top of the boundary layer in the nonlinear solution shows inertial oscillations that are an unrealistic feature of the nonlinear slab boundary-layer model. These oscillations are a manifestation of the only physical process by which the boundary layer can adjust to the radially changing gradient wind profile at its top in the slab model (Smith and Vogl, 2008; Kepert, 2012) and as seen in Figure 5(b), they are filtered out in the linear solution.

The radial inflow in the boundary layer is generally weak (less than 0.5 m s^{-1}) and decreases in strength with decreasing radius from about 175 km. The increasing magnitude of u_b with decreasing radius is accompanied at large radii by an increase in the rate of subsidence at the top of the boundary layer. At radii less than about 210 km, the vertical velocity at the top of the boundary layer (w_b) becomes positive and reaches a maximum of nearly 5 mm s^{-1} at a radius of about 85 km. Even though this may seem weak, it would lead to a vertical displacement of air parcels of more than 200 m in 12 h, sufficient to have a significant impact on reducing the local CIN. Indeed, the boundary-layer induced ascent provides a suitable region for deep convection to develop and focus. As the vortex wind field strengthens and expands, the moisture will increase within the boundary layer, and the ascent will increase in strength at the top of the boundary layer. In this way the boundary layer exerts a progressive control on the inner core convection as the vortex intensifies (Kilroy *et al.*, 2016a).

In the absence of boundary-layer friction, deep convection develops without any systematic organization and lies often outside the radius of maximum tangential winds.

6. Spin-up in the simulation without friction

Despite the lack of convective organization driven by boundary-layer dynamics, the vortex in Ex-NoFr does eventually spin up (Figure 1(a)). The vortex intensifies gradually over time until about 108 h, after which, the intensification rate increases markedly. It was shown in KSM for Ex-Fr that prior to any noticeable increase in V_{max} (before the intensification begin time at 45 h), there was persistent deep convection occurring near the circulation centre. This deep convection acts to amplify vertical vorticity in the inner core via vortex tube stretching. The system-scale inflow associated with the deep convection converges vertical vorticity radially inwards, thereby increasing the local circulation. By this process, a monolithic core of strong cyclonic vorticity has formed just before RI. In this section we perform a similar

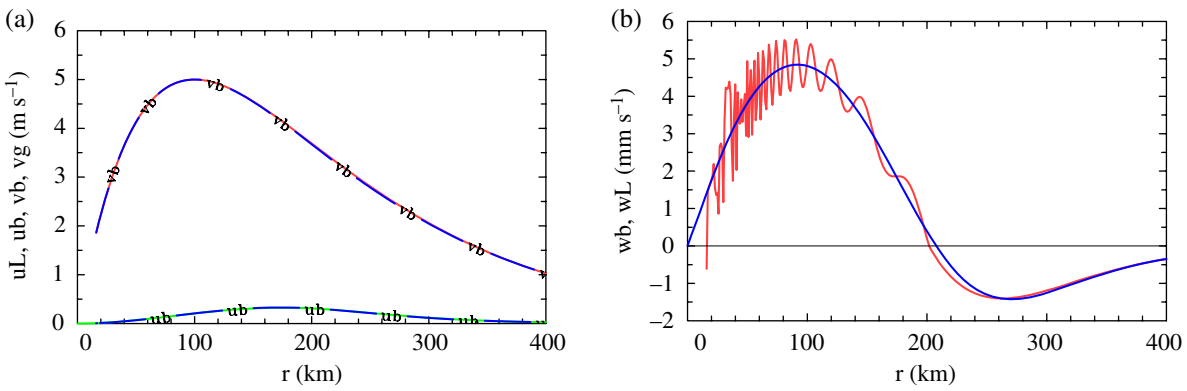

Figure 5. (a) Radial profiles of radial and tangential wind components, u_b and v_b respectively, in the boundary layer (blue curves) for a fixed profile of gradient wind at the top of the boundary layer (the red line partially hidden). The green line (partially hidden) shows the radial inflow in the linear solution for the boundary layer. (b) shows the corresponding profiles of vertical velocity at the top of the boundary layer calculated from the nonlinear (red curve) and the linear (blue curve) solutions. The calculations are based on the assumption of a constant boundary-layer depth of 1 km at a radius of 500 km. [Colour figure can be viewed at wileyonlinelibrary.com].

analysis for the inner core region of Ex-NoFr at various times prior to intensification.

To investigate how vertical vorticity accumulates in the inner core in Ex-NoFr, we show in Figure 6 horizontal cross-sections of vertical vorticity, wind vectors at a height of 1 km, and surface pressure at various times from 45 to 132 h. Contours of vertical velocity equal to 1 m s^{-1} at heights of 2 and 6 km are superimposed to indicate the location of strong updraughts at these levels.

KSM identified 45 h as the intensification begin time for Ex-Fr (their figure 3b). At that time the inner 20 km × 20 km grid is engulfed by deep convection and there are numerous patches of cyclonic vertical vorticity surrounding this area. At 45 h in Ex-NoFr, the situation is vastly different (Figure 6(a)). At this time there are only two active convective cells in the inner 100 km × 100 km grid, while there are a few sparsely located patches of vertical vorticity. By 90 h there are some patches of cyclonic vorticity near the circulation centre, although interestingly, deep convection at no time occurs near the circulation centre (not shown). The reason for the lack of convection is presumably because of the large CIN and enhanced drying that occurs in the inner 20 km × 20 km column (Figures 4(a) and (c)). Nonetheless, patches of enhanced vertical vorticity have migrated into this region by 90 h. There is a decrease also in surface pressure as depicted by the black contour in Figure 6.

At 108 h (Figure 6c), V_{max} begins to increase with time more rapidly (Figure 1(a)). At this time there are many active deep convective cells with associated patches of enhanced vertical vorticity, although these convective cells are mostly located away from the circulation centre. The surface pressure has dropped further and VT_{max} has increased by 4.3 m s^{-1} compared to 90 h. Once again a main feature at this time is the lack of deep convection near the circulation centre. Indeed, the innermost 30 km ×30 km centred on the circulation centre contains very little active convection. Despite this, the area of enhanced vertical vorticity in this region continues to grow.

At 120 h (Figure 6d), the situation is similar to 12 h earlier in terms of the location of deep convection. By this time, VT_{max} is now 26.7 m s^{-1}. The number of deep convective cells has increased since 108 h, although once again, these cells are located far away (about 20 km) from the circulation centre. The convection is beginning to develop into an eyewall structure, at a radius of about 40 km, which coincides with the radius of maximum winds at this time (Figure 1(b)). The strongest patches of cyclonic vorticity ($> 1 \times 10^{-3}$s^{-1}) are located in or near the eyewall region, although the circulation centre has relatively low values of vertical vorticity at this time.

At 132 h (Figure 6e), there is a strong increase in both V_{max} and VT_{max} (Figure 1(a)). The horizontal structure of the system has changed markedly from 12 h before and a more coherent ring-like structure in the vorticity field has emerged. During this time there has been a continual migration of patches of enhanced cyclonic vorticity towards the circulation centre, despite the absence of deep convection there. Over the next 24 h the vorticity within the ring continues to increase with values exceeding 2×10^{-3}s^{-1}, despite the continued lack of convection in that region.

While observing the vorticity evolution of the zero drag simulation, there appears to be several barotropic-like mechanisms in action: vorticity anomalies move upgradient until the ring of vorticity forms. This upgradient vorticity transfer is consistent with the theories of Schecter and Dubin (1999), McWilliams *et al.* (2003) and Montgomery and Enagonio (1998). However, to explain the large values of vertical vorticity that continue to migrate towards the circulation centre within the ring-like configuration, a different mechanism needs to be invoked. As explained by Schubert *et al.* (1999), rings of vorticity have the propensity to become barotropically unstable and the mixing that ensues can lead to the maximum vorticity migrating inwards. While the stronger regions of cyclonic vorticity in Schubert *et al.* (1999) underwent a weakening as the ring transformed into a monopole, the ring of vorticity in Ex-NoFr is continually reinforced by the generation of cyclonic vorticity anomalies outside the ring, which then move updradient into the ring as described above. These proffered explanations, which are all based on barotropic dynamics, offer a plausible zero-order interpretation of the upscaling of vorticity near the circulation centre in the absence of friction. A further investigation of these processes is certainly warranted, but falls beyond the scope of this paper.

In summary, we have highlighted some major differences between simulations with and without surface friction. Namely, without boundary-layer dynamics determining where the upflow out of the boundary layer must occur, deep convection is unfocused and occurs at large radii. The collective effects of the convection occurring at large radii is to force subsidence, and drying, in the inner core region, increasing the CIN there and making the inner core less susceptible to convection. Eventually, as convection occurs inside the radius of maximum winds, spin-up occurs as M-surfaces are drawn gradually inwards below and above the boundary layer. In the absence of friction, these surfaces are approximately materially conserved within the thermodynamic boundary layer also. Despite the fact that deep convection never occurs close to (within 30 km radius of) the circulation centre, patches of enhanced vertical vorticity gradually migrate to the centre over time, eventually filling the inner core with large values of cyclonic vertical vorticity. This result suggests the importance of barotropic-like dynamics in the absence of surface friction. When surface friction is included, the inflow generated within the boundary layer plays, in part, a role in merging patches of enhanced vertical vorticity on a much shorter time-scale (KSM).

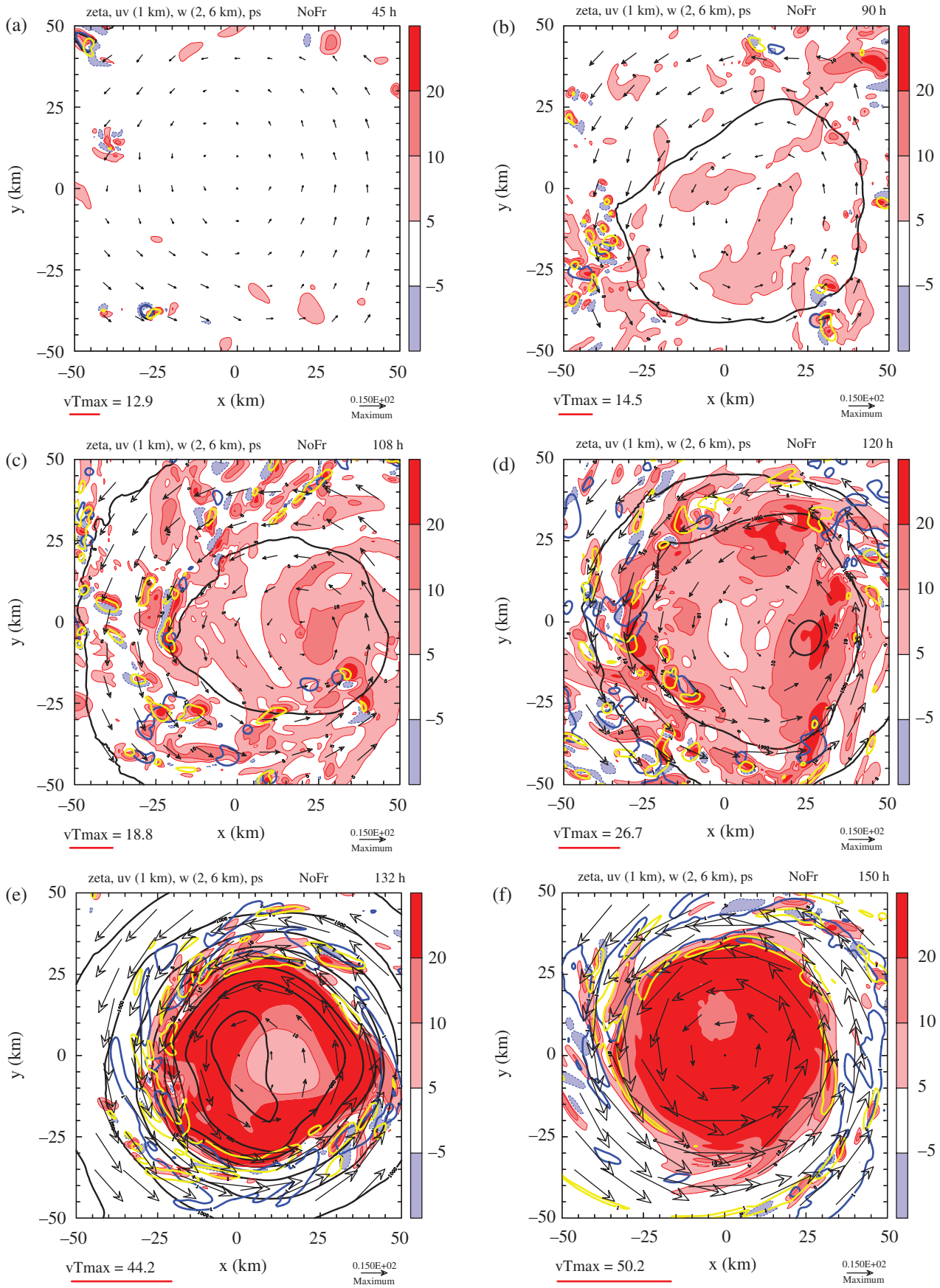

Figure 6. Horizontal cross-sections of relative vertical vorticity (shading, multiplied by 10^{-4}) and wind vectors at (a) 45 h, (b) 90 h, (c) 108 h, (d) 120 h, (e) 132 h, and (f) 156 h at 1 km altitude for Ex-NoFr. Also shown are contours of vertical velocity (contour interval 1 m s^{-1}) at heights of 2 km (aqua) and 6 km (yellow), and of surface pressure (black) contoured every 2 hPa. The wind vectors are relative to the maximum reference vector at the bottom right, while the maximum total wind speed in the domain plotted is given in m s^{-1} at the bottom left.

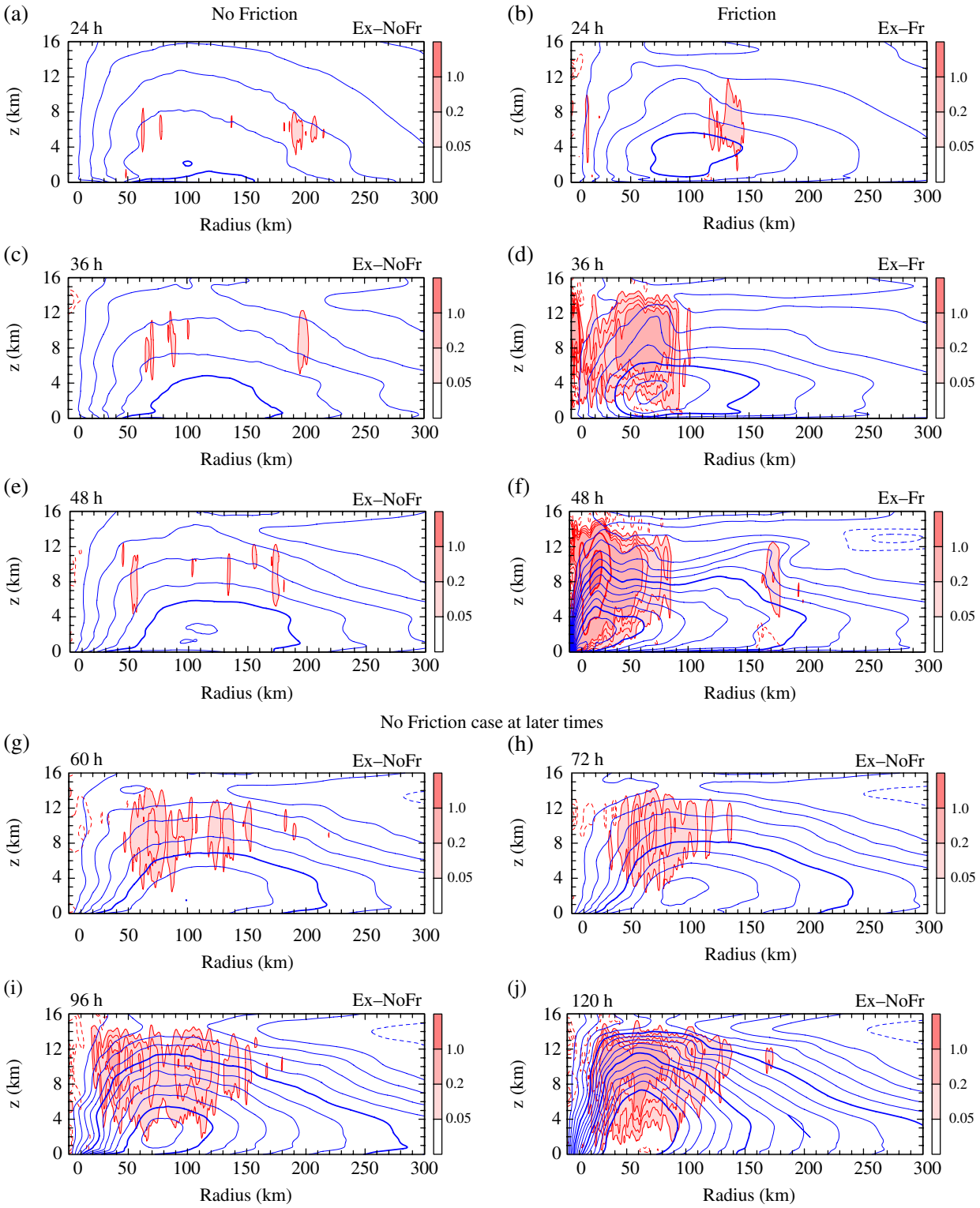

Figure 7. Vertical cross-sections of the azimuthally averaged, 3 h time-averaged tangential component of velocity (contours) centred at (a, b) 24 h (c, d) 36 h, (e, f) 48 h in the two experiments. (g)–(j) show the NoFr case at later times (g) 60 h, (h) 72 h, (i) 96 h, and (j) 120 h. Also shown is the averaged vertical velocity (shading). Contours are: tangential velocity (thin blue, 1 m s^{-1} interval between 0 and 15 m s^{-1}, thick blue every 5 m s^{-1}), vertical velocity (thin red contours every 0.05 m s^{-1} to 0.2 m s^{-1}, thick red every 0.5 m s^{-1}). Thin dashed red contours indicate subsidence at intervals of 0.02 m s^{-1}. [Colour figure can be viewed at wileyonlinelibrary.com].

7. An azimuthally averaged view of vortex evolution

In section 3 we described the behaviour of various metrics characterizing the behaviour of the azimuthally averaged state. We examine now the evolution of the azimuthally averaged flow structure. Figures 7(a)–(f) compare vertical cross-sections of the azimuthally averaged, 3 h time-averaged tangential velocity and vertical velocity in Ex-NoFr (left panels) and Ex-Fr (right panels) at 24, 36 and 48 h, while (g)–(j) show the further evolution in Ex-NoFr to 120 h. The time averaging is centred on the time shown.

It is clear from these fields that the evolution of the vortex in Ex-NoFr is quite different to that in Ex-Fr. In particular, in the early stages, deep convection as reflected in the vertical velocity field shows strong organization in Ex-Fr, even by 36 h and, as a result, the tangential wind field has begun to intensify and spread radially. In contrast, in Ex-NoFr, the convection shows no sign of organization. Even by 48 h, the tangential wind field has barely changed, the maximum having increased by little more than 1 m s^{-1} from its initial state, whereas, in Ex-Fr at this time, the maximum has increased to about 13 m s^{-1}.

By 48 h, the vortex in Ex-Fr has begun to rapidly intensify, whereas, as seen in Figures 7(g)–(j), the vortex in Ex-NoFr

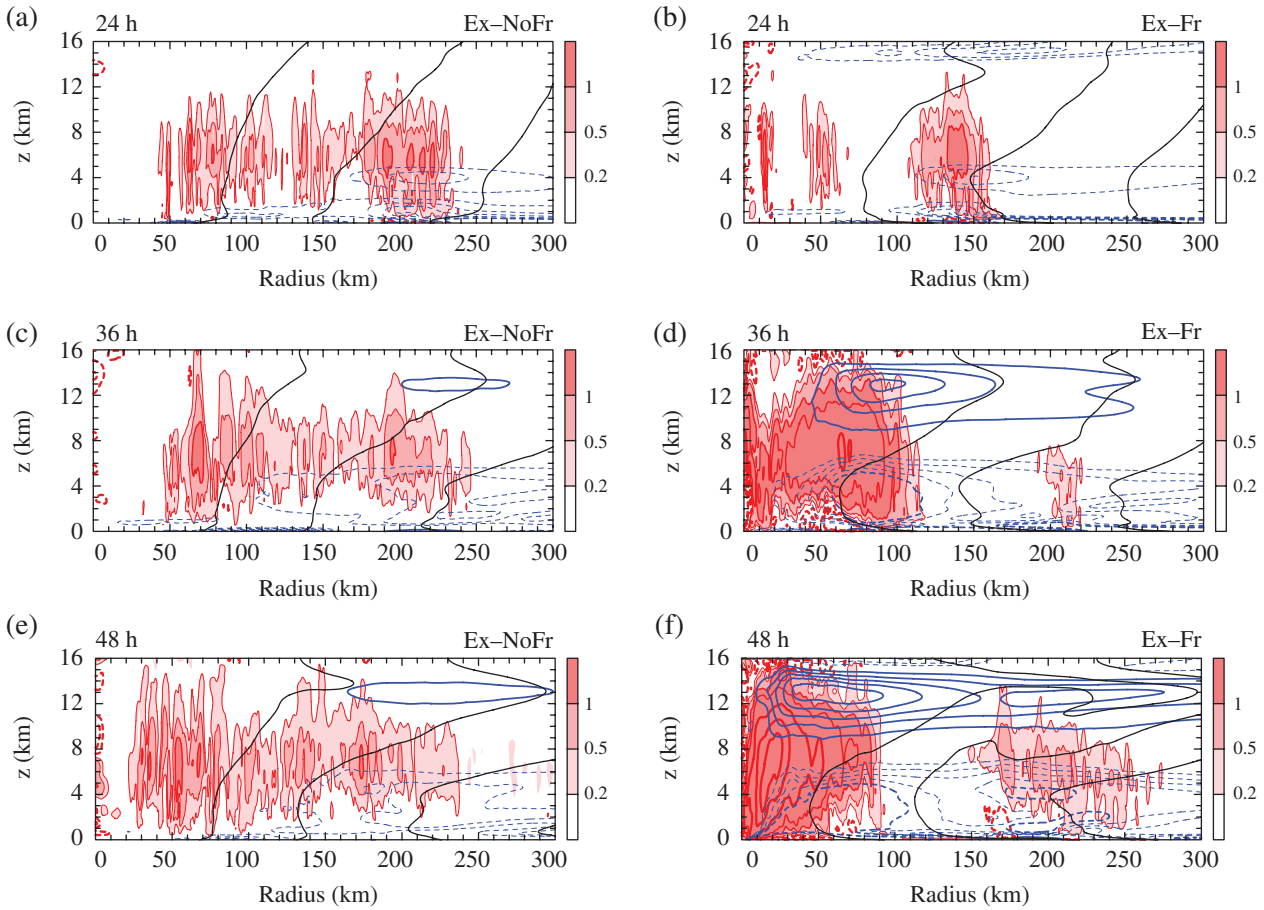

Figure 8. Vertical cross-sections of the azimuthally averaged, 3 h time-averaged radial velocity component centred at at (a, b) 24 h (c, d) 36 h, (e, f) 48 h in the two experiments. Superimposed on the radial component is the averaged diabatic heating rate with some shading as indicated and selected contours of absolute angular momentum. Contours are: radial velocity (thick blue contours every 1 m s^{-1}, dashed negative, thin blue dashed contours every 0.2 m s^{-1} down to −0.8 m s^{-1}), diabatic heating rate (thin red contours 0.2 and 0.5 K day^{-1}, dashed negative, medium thickness red contours 1 and 2 K day^{-1}, thick red contours every 5 K day^{-1}), absolute angular momentum (thick black contours every 5×10^5 m^{2}s^{-1}). [Colour figure can be viewed at wileyonlinelibrary.com].

develops only slowly for another three days. At 120 h, the maximum tangential wind speed is about 15 m s^{-1} at a radius of 55 km. While the vortex intensifies beyond this time, it does not become appreciably more compact, the minimum value of R_{vmax} does not decrease much below 40 km (Figure 1).

Figure 8 compares vertical cross-sections of the azimuthally averaged, 3 h time-averaged, radial velocity u, diabatic heating rate $\dot{\theta}$, and absolute angular momentum M at 24, 36 and 48 h in Ex-NoFr and Ex-Fr. Again, the rapid organization of deep convection, characterized here by the highly localized diabatic heating distribution, is evident in Ex-Fr, whereas the absence of such organization is a feature of the Ex−NoFr simulation during the same time period. The organization of convection in Ex-Fr is accompanied by much stronger inflow in the lower troposphere and therefore a much greater inward radial displacement of the M-surfaces than in Ex-NoFr. This displacement is consistent, of course, with the larger tangential velocities seen in Figures 7(b), (d) and (f).

While some of the low-level inflow seen in Figures 8(b), (d) and (f) may be attributed to the 'sucking effect' of deep convection, the organization of the convection in Ex-Fr, as described in the preceding section, has no counterpart in Ex-NoFr. This organization in Ex-Fr is associated with the boundary-layer induced inflow. As noted by Smith and Montgomery (2015), it is not possible, in general, to isolate analytically the separate effects of deep convection and boundary-layer friction in producing inflow in the boundary layer. This is because of the intrinsic nonlinearity of the boundary layer when the characteristic vortex Rossby number becomes of order unity (Smith and Montgomery, 2008; Vogl and Smith, 2009; Montgomery *et al.*, 2014). However it is possible to estimate the boundary-layer contribution as articulated by Kilroy *et al.* (2016a) and it is possible to estimate the inflow induced by deep convection in the absence of friction by doing a balance calculation[††].

In the Ex-NoFr calculation, the balance calculation should be good everywhere, at least for the azimuthally averaged flow, and therefore helpful in interpreting the subsequent evolution beyond 48 h. For this reason we show in Figure 9 similar figures to those in the left column of Figure 8, but for later times to 120 h, together with the corresponding balance calculations in the right column. The balance calculations for the radial velocity component are based on a solution of the Sawyer−Eliassen equation for the streamfunction of the secondary circulation as discussed in Kilroy *et al.* (2016a)[‡‡]. Comparison of the radial velocity component in the full solution and in the corresponding axisymmetric Eliassen balance solution (forced by the time and azimuthally averaged diabatic heating rate) shows quantitatively good agreement, supporting the interpretation that, without friction, the azimuthally averaged transverse circulation is captured largely by axisymmetric balance dynamics.

From an azimuthally averaged perspective, in the friction run, the strongest azimuthally averaged tangential wind speed occurs in the frictional boundary layer (Kilroy *et al.*, 2017, their figure 6 at 48 h and beyond) as a result of the boundary-layer spin-up mechanism (Smith *et al.*, 2009). In the no-friction simulation, the

[††]One can estimate the boundary-layer contribution of deep convection in a balance calculation also, but because the boundary layer is generally not close to balance in the inner core of tropical cyclones, this estimate is unlikely to be robust (e.g. Smith *et al.*, 2009).

[‡‡]As in Kilroy *et al.*, the radial resolution of the streamfunction calculation was degraded to facilitate convergence of the solution using an iterative successive over-relaxation method in a reasonable time. Specifically the calculation was carried out on a domain 500 km in radius and 16 km high with open boundary condition on the streamfunction at the far radius.

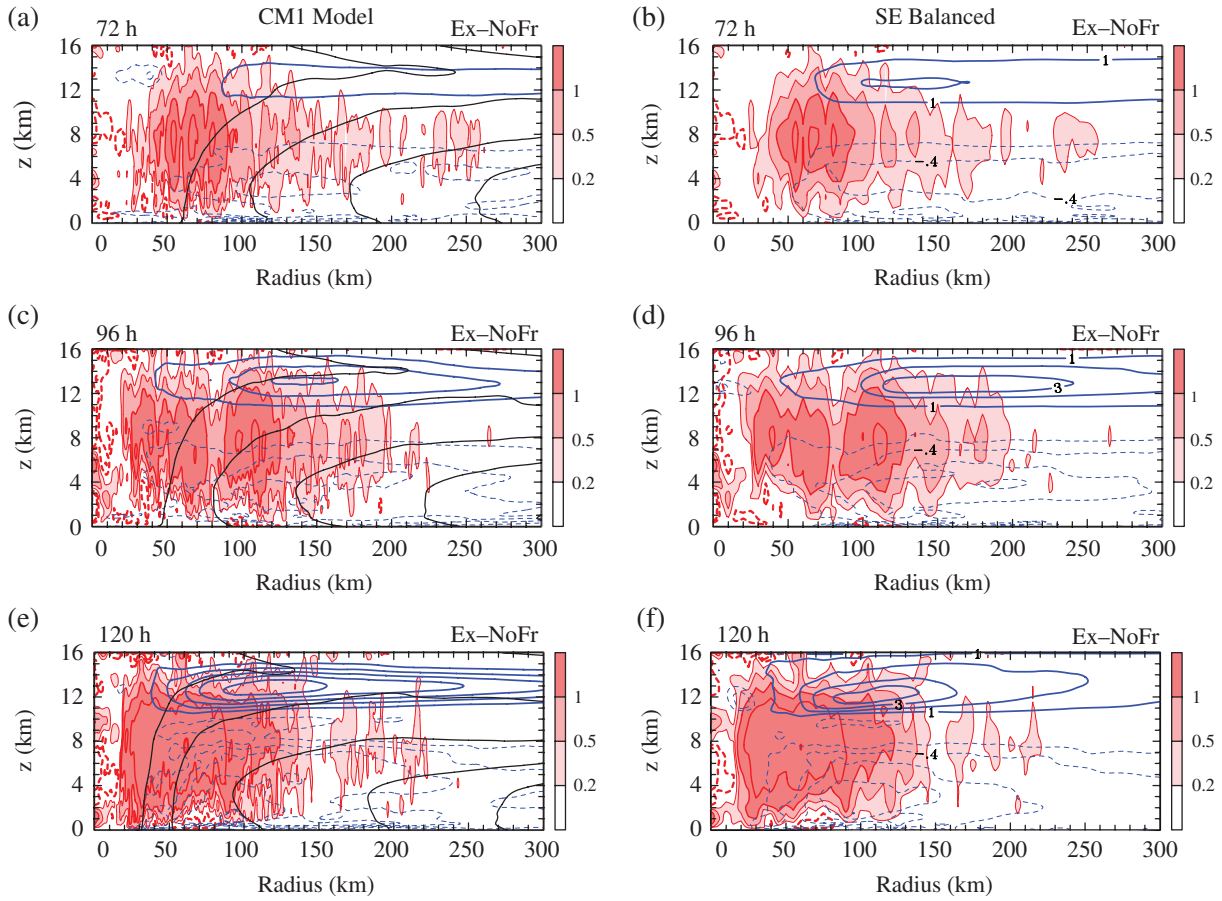

Figure 9. Radius–height cross-sections similar to Figures 8(b, d, f), but showing the filtered diabatic heating rate and the balanced radial flow calculated from the solution of the Sawyer–Eliassen equation forced by this heating distribution. Contours of absolute angular momentum are not shown again in the balanced plots (b, d, f). Contour information is as in Figure 8. [Colour figure can be viewed at wileyonlinelibrary.com].

maximum tangential wind speed can occur at mid-levels or low-levels (Figure 7), and M is approximately materially conserved at all locations as there is no boundary layer. The primary reason for weaker winds in the no-friction run is that, because there is no focussing of the convection near the circulation centre, the eyewall that eventually develops is located much further out radially than in the friction run (R_{vmax} plot in Figure 1). Even though M is approximately materially conserved at all locations in Ex-noFr, since the 'eyewall' is located much further out, the M-surfaces are not drawn as close to the centre as in Ex-Fr.

8. Relation to previous work

The findings from sections 5 and 6 are believed to be significant because they offer new insights on the role of surface friction in fostering convective organization in the vortex development process and they offer also new insight on the mechanism of vortex spin-up without surface friction. Previous studies by Schecter (2011) and Bryan (2012) have considered, *inter alia*, the influence of surface friction on vortex development and the relation of these studies to the present one will be discussed here.

As part of an effort to evaluate a family of reduced models for tropical cyclone behaviour, Schecter (2011) conducted high-resolution, near-cloud-resolving simulations of tropical cyclogenesis starting from small-amplitude turbulence in the wind field within a convectively favourable, quiescent environment. He found that by suppressing surface drag entirely, the lack of boundary-layer convergence inhibits cyclone formation. In particular, with zero surface drag, he found that there was no sign of cyclone formation during a 30 day simulation. Moreover, as noted in the Introduction, consistent with Persing *et al.* (2013), Schecter (section 2.2) noted that 'the influence of surface drag remains minimal 7.33 days into genesis, but seems to nudge convection toward the centre of the developing domain-scale circulation'. Although we have not tried to duplicate his results exactly, our results support his findings in the sense that friction provides a mechanism for helping convection focus near the circulation centre. In contrast to the results of Schecter, our experiment without friction eventually predicts spin-up, but on a relatively long time-scale. Of course, there are differences between our set-up and his, namely, we employ a higher SST (29°C versus 26°C), a relatively moist 'pouch sounding' two days prior to the formation of tropical storm *Karl* during the PREDICT experiment, etc. (section 2 gives details), and we employ a single vortex as initial condition while he starts from a turbulent initial condition with a specified energy spectra. Moreover, he uses a different numerical model with much coarser horizontal grid spacing (3.9 km versus 500 m used here). The differences in the thermodynamics might plausibly account for the eventual spin-up found here without friction. Nevertheless, there appears to be consensus of both studies that surface friction plays an important role at early times in the development process.

The explanation for vortex intensification in the absence of surface drag offered in the previous section is in contrast to that given by Bryan (2012). His interpretation of spin-up without drag invokes the vertical redistribution of tangential momentum near the surface to higher levels by the turbulence scheme. He explains that 'because v [defined as the azimuthally averaged tangential velocity: our insertion] decreases with height in the initial conditions, the turbulence model would act to decrease v near the surface (and increase v aloft). Assuming the radial pressure gradient stays roughly the same, this decrease in v near the surface can lead to radial inflow and thus intensification.' Figure 10(a) shows the initial vortex wind structure along with the corresponding M-surfaces, while (b) and (c) show the corresponding vortex structure at 5 h in Ex-NoFr and Ex-Fr, respectively. The initial vortex structure has an almost zero vertical gradient in both v and M in the lowest 2 km, suggesting that there would be minimal reduction of v by the turbulence

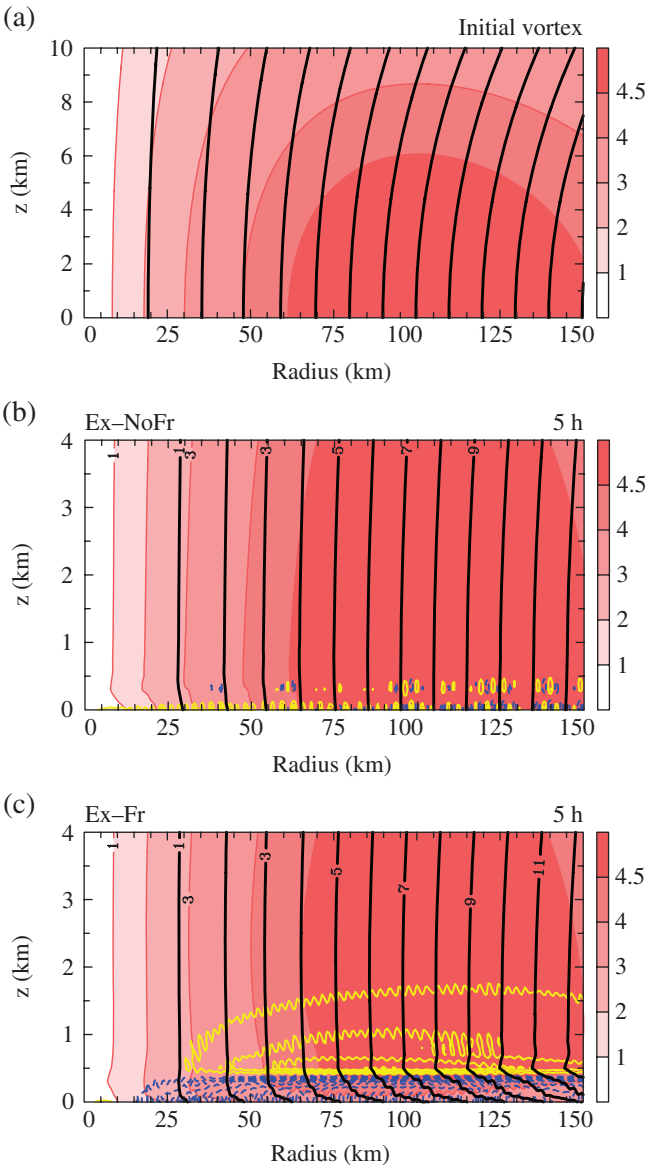

Figure 10. Vertical cross-section of (a) the initial vortex structure, and the vortex structure at 5 h in (b) Ex-NoFr and (c) Ex-Fr. The V wind component appears as contours with shading; contours of the radial component of velocity are from $\pm 0.1\,\mathrm{m\,s^{-1}}$ to $\pm 1.0\,\mathrm{m\,s^{-1}}$ at intervals of $0.1\,\mathrm{m\,s^{-1}}$. Inflow contours are dashed blue, outflow are solid yellow. Absolute angular momentum is shown as black contours every $1 \times 10^{-7}\,\mathrm{m^2\,s^{-1}}$. [Colour figure can be viewed at wileyonlinelibrary.com].

scheme in this layer. Furthermore, we find that there is no development of systematic inflow in Ex-NoFr near the surface at 5 h (Figure 10(b)) or before the initial burst of deep convection at about 12 h (not shown). In fact, in the lowest few hundred metres above the surface, there is mostly weak disorganised outflow, leading to weak outward-sloping M-surfaces there. In Ex-Fr (Figure 10(c)) the vortex structure is fundamentally different, with a layer of relatively strong inflow (maximum magnitude of $0.94\,\mathrm{m\,s^{-1}}$) to a depth of 500 m, with weak outflow above that.

In conclusion, we find no supporting evidence of the turbulence scheme playing any significant role in generating inflow or spinning up the vortex in Ex-NoFr*.

In a recent study, Heng and Wang (2016) carried out a pair of numerical model simulations, one with and the other without surface drag, but with the same fixed distribution of heating to force the intensification of a prescribed initial vortex. They found that the vortex in the case without surface drag became the more intense. This is just the opposite to the finding of the present study. The implication is, of course, that the diabatic heating rate cannot be presumed to be the same as it will depend on the details of the evolving field of convection, which is, as we have shown, tied to the dynamics and thermodynamics of the evolving boundary layer. In the absence of a boundary layer in the case without surface drag, the only influence on the location of the convection is the pattern of enhanced surface moisture fluxes in the vicinity of the maximum tangential wind of the vortex. It follows that the assumption of the same fixed heating distribution in the Heng and Wang simulations provides an unrealistic thought experiment in their words (p. 1318), '... to clarify the recent debate on the role of surface friction in tropical cyclone intensification'.

9. Conclusions

To investigate the effects of surface friction during tropical cyclogenesis, we have compared the results of two idealized, high-resolution, numerical model simulations, one with and one without surface drag. While spin-up occurs in both simulations, the vortex in the one without surface drag takes over twice as long to reach its intensification begin time. Further, the simulated vortex is considerably larger in inner core size and weaker in intensity.

A major difference between the two simulations is that there is no mechanism to focus deep convection close to the circulation centre in the simulation without friction. The frictional boundary-layer dynamics play an important role in focusing the convection near the circulation centre, which then increases the moisture in that region. Indeed, the boundary-layer induced ascent provides a suitable region for deep convection to develop and focus. As the tangential wind field of the vortex strengthens and expands, the moisture increases within the boundary layer, and the ascent increases in strength at the top of the boundary layer. In this way the boundary layer exerts a progressive control on the inner core convection as the vortex evolves.

In the absence of friction, deep convection is unfocused and at early times occurs predominantly at large radii, where surface fluxes are a maximum. The collective effects of this convection is to force subsidence, and drying, in the inner core region, increasing the CIN there and making the inner core less susceptible to convection. Eventually, as convection develops inside the radius of maximum winds, spin-up occurs as M-surfaces are drawn gradually inwards within and above the boundary layer.

Without friction, the M-surfaces are materially conserved within the thermodynamic boundary layer also. However, despite the fact that deep convection never occurs close to (within 30 km radius of) the circulation centre, patches of enhanced vertical vorticity gradually migrate towards the centre to form a monopole of cyclonic vertical vorticity. These findings suggest the importance of barotropic-like vorticity dynamics in the absence of surface friction. In contrast, when surface friction is included, the inflow generated within, and above, the boundary layer plays a larger role in the merger of patches of enhanced cyclonic vorticity on a much shorter time-scale.

A comparison of the radial velocity component in the full solution with that in the corresponding axisymmetric Eliassen balance solution (forced by the time and azimuthally averaged diabatic heating rate) shows quantitatively good agreement, supporting the interpretation that, without friction, the azimuthally averaged transverse circulation is captured largely by axisymmetric balance dynamics.

*In view of the intrinsic limitations of strictly axisymmetric modelling for tropical cyclone intensification found by Persing *et al.* (2013), it should be noted that there may be inherent differences in the spin-up of the zero-drag, three-dimensional, simulation presented here and in the axisymmetric, zero-drag simulation of Bryan (2012). However, on account of the near-zero vertical gradient of tangential wind near the surface for the initial vortex used here, we hypothesize that the vortex will not spin up in an axisymmetric zero-drag simulation by the pathway suggested by Bryan (2012). This issue warrants further study.

Relating our work to some notable previous studies, we find that there is now an emerging consensus that surface friction plays an important role at early times in the tropical cyclogenesis process. We find no supporting evidence of the turbulence scheme playing any significant role in generating inflow or in spinning up the vortex in our simulations. Consistent with recent work, the results demonstrate that the convective organization process is aided by frictional convergence and raise the possibility that the timing of genesis in numerical models may depend on the boundary-layer parametrization scheme. This would seem to be a topic that merits further investigation.

In summary, in the absence of boundary-layer friction, the convection eventually develops without any systematic organization and lies often outside the radius of azimuthally averaged maximum tangential winds. The results underscore the crucial role of friction in organizing deep convection in the inner core of the nascent vortex. Moreover, they point to the danger of comparing simulations with and without friction using the same *prescribed* diabatic heating rate as was done by Heng and Wang (2016) in an attempt to downplay the role of friction in the intensification process.

Acknowledgements

We thank Kerry Emanuel, Yuqing Wang and an anonymous reviewer for their thoughtful reviews of the original manuscript. GK and RKS acknowledge financial support for tropical cyclone research from the German Research Council (Deutsche Forschungsgemeinschaft) under grant numbers SM30/23-3 and SM30/23-4 and the Office of Naval Research Global under grant no. N62909-15-1-N021. MTM acknowledges the support of NSF grant AGS-1313948, NOAA HFIP grant N0017315WR00048, NASA grant NNG11PK021 and the US Naval Postgraduate School.

References

Anthes RA. 1974. The dynamics and energetics of mature tropical cyclones. *Rev. Geophys. Space Phys.* **12**: 495–522.

Bryan GH. 2012. Comments on 'Sensitivity of tropical-cyclone models to the surface drag coefficient'. *Q. J. R. Meteorol. Soc.* **139**: 1957–1960.

Bryan GH, Fritsch JM. 2002. A benchmark simulation for moist nonhydrostatic numerical models. *Mon. Weather Rev.* **130**: 2917–2928.

Bryan GH, Rotunno R. 2009. The maximum intensity of tropical cyclones in axisymmetric numerical model simulations. *Mon. Weather Rev.* **137**: 1770–1789.

Carrier GF. 1971. Swirling flow boundary layers. *J. Fluid Mech.* **49**: 133–144.

Charney JG, Eliassen A. 1964. On the growth of the hurricane depression. *J. Atmos. Sci.* **21**: 68–75.

Cotton WR, Pielke RA, Walko RL, Liston GE, Tremback CJ, Jiang H, McAnelly RL, Harrington JY, Nicholls ME, Carrio GG, McFadden JP. 2013. RAMS 2001: Current status and future directions. *Meteorol. Atmos. Phys.* **82**: 5–29.

Craig GC, Gray SL. 1996. CISK or WISHE as a mechanism for tropical cyclone intensification. *J. Atmos. Sci.* **53**: 3528–3540.

Črnivec N, Smith RK, Kilroy G. 2016. Dependence of tropical cyclone intensification rate on sea surface temperature. *Q. J. R. Meteorol. Soc.* **142**: 1618–1627.

Emanuel KA. 1986. An air–sea interaction theory for tropical cyclones. Part I: Steady state maintenance. *J. Atmos. Sci.* **43**: 585–604.

Emanuel KA. 1989. The finite amplitude nature of tropical cyclogenesis. *J. Atmos. Sci.* **46**: 3431–3456.

Emanuel KA. 1995. Sensitivity of tropical cyclones to surface exchange coefficients and a revised steady-state model incorporating eye dynamics. *J. Atmos. Sci.* **52**: 3969–3976.

Emanuel KA. 1997. Some aspects of hurricane inner-core dynamics and energetics. *J. Atmos. Sci.* **54**: 1014–1026.

Heng J, Wang Y. 2016. Nonlinear response of a tropical cyclone vortex to prescribed eyewall heating with and without surface friction in TCM4: Implications for tropical cyclone intensification. *J. Atmos. Sci.* **73**: 1315–1333.

Kaplan J, DeMaria M. 2003. Large-scale characteristics of rapidly intensifying tropical cyclones in the North Atlantic Basin. *Weather Forecasting* **18**: 1093–1108.

Kepert JD. 2012. Choosing a boundary-layer parameterisation for tropical cyclone modelling. *Mon. Weather Rev.* **140**: 1427–1445.

Kilroy G, Smith RK. 2016a. Why do model tropical cyclones grow progressively in size and decay in intensity after reaching maturity? *J. Atmos. Sci.* **73**: 487–503.

Kilroy G, Smith RK, Montgomery MT, Lynch B, Earl-Spurr C. 2016b. A case-study of a monsoon low that formed over the sea and intensified over land as seen in the ECMWF analyses. *Q. J. R. Meteorol. Soc.* **142**: 2244–2255.

Kilroy G, Smith RK, Montgomery MT. 2017. A unified view of tropical cyclogenesis and intensification. *Q. J. R. Meteorol. Soc.* **143**: 450–462.

McWilliams JC, Graves LP. 2003. A formal theory for vortex Rossby waves and vortex evolution. *Geophys. Astrophys. Fluid Dyn.* **97**: 275–309.

Montgomery MT, Enagonio J. 1998. Tropical cyclogenesis via convectively forced vortex Rossby waves in a three-dimensional quasi-geostrophic model. *J. Atmos. Sci.* **55**: 3176–3207.

Montgomery MT, Smith RK. 2017. Recent developments in the fluid dynamics of tropical cyclones. *Annu. Rev. Fluid Mech.* **49**: 1–33.

Montgomery MT, Nicholl ME, Cram TA, Saunders A. 2006. A 'vortical' hot tower route to tropical cyclogenesis. *J. Atmos. Sci.* **63**: 355–386.

Montgomery MT, Smith RK, Nguyen SV. 2010. Sensitivity of tropical cyclone models to the surface drag coefficient. *Q. J. R. Meteorol. Soc.* **136**: 1945–1953.

Montgomery MT, Davis C, Dunkerton T, Wang Z, Velden C, Torn R, Majumdar SJ, Zhang F, Smith RK, Bosart L, Bell MM, Haase JS, Heymsfield A, Jensen J, Campos T, Boothe MA. 2012. The Pre-Depression Investigation of Cloud Systems in the Tropics (PREDICT) Experiment: Scientific basis, new analysis tools and some first results. *Bull. Am. Meteorol. Soc.* **93**: 153–172.

Montgomery MT, Zhang JA, Smith RK. 2014. The low-level structure of rapidly intensifying and mature hurricane *Earl*. *Q. J. R. Meteorol. Soc.* **140**: 2132–2146.

Ooyama KV. 1969. Numerical simulation of the life cycle of tropical cyclones. *J. Atmos. Sci.* **26**: 3–40.

Ooyama KV. 1982. Conceptual evolution of the theory and modeling of the tropical cyclone. *J. Meteorol. Soc. Jpn.* **60**: 369–380.

Persing J, Montgomery MT, McWilliams J, Smith RK. 2013. Asymmetric and axisymmetric dynamics of tropical cyclones. *Atmos. Chem. Phys.* **13**: 12249–12341.

Rosenthal SL. 1971. The response of a tropical cyclone model to variations in boundary-layer parameters, initial conditions, lateral boundary conditions, and domain size. *Mon. Weather Rev.* **99**: 767–777.

Rotunno R, Emanuel KA. 1987. An air–sea interaction theory for tropical cyclones. Part II: Evolutionary study using a non-hydrostatic axisymmetric numerical model. *J. Atmos. Sci.* **44**: 542–561.

Schecter DA. 2011. Evaluation of a reduced model for investigating hurricane formation from turbulence. *Q. J. R. Meteorol. Soc.* **137**: 155–178.

Schecter DA, Dubin DHE. 1999. Vortex motion driven by a background vorticity gradient. *Phys. Rev. Lett.* **83**: 2191–2194.

Schecter DA, Dunkerton TJ. 2009. Hurricane formation in diabatic Ekman turbulence. *Q. J. R. Meteorol. Soc.* **135**: 823–838.

Schmidt CW, Smith RK. 2016. Tropical cyclone evolution in a minimal axisymmetric model revisited. *Q. J. R. Meteorol. Soc.* **142**: 1505–1516.

Schubert WH, Montgomery MT, Taft RK, Guinn TA, Fulton SR, Kossin JP, Edwards JP. 1999. Polygonal eyewalls, asymmetric eye contraction, and potential vorticity mixing in hurricanes. *J. Atmos. Sci.* **56**: 1197–1223.

Smith RK, Montgomery MT. 2008. Balanced boundary layers used in hurricane models. *Q. J. R. Meteorol. Soc.* **134**: 1385–1395.

Smith RK, Montgomery MT. 2012. Observations of the convective environment in developing and non-developing tropical disturbances. *Q. J. R. Meteorol. Soc.* **138**: 1721–1739.

Smith RK, Montgomery MT. 2015. Towards clarity on understanding tropical cyclone intensification. *J. Atmos. Sci.* **72**: 3020–3031.

Smith RK, Montgomery MT. 2016a. Understanding hurricanes. *Weather* **71**: 219–223.

Smith RK, Montgomery MT. 2016b. The efficiency of diabatic heating and tropical cyclone intensification. *Q. J. R. Meteorol. Soc.* **142**: 2081–2086.

Smith RK, Vogl S. 2008. A simple model of the hurricane boundary layer revisited. *Q. J. R. Meteorol. Soc.* **134**: 337–351.

Smith RK, Montgomery MT, Nguyen SV. 2009. Tropical cyclone spin-up revisited. *Q. J. R. Meteorol. Soc.* **135**: 1321–1335.

Smith RK, Montgomery MT, Thomsen G. 2014. Sensitivity of tropical cyclone models to the surface drag coefficient in different boundary-layer schemes. *Q. J. R. Meteorol. Soc.* **140**: 792–804.

Smith RK, Kilroy G, Montgomery MT. 2015a. Why do model tropical cyclones intensify more rapidly at low latitudes? *J. Atmos. Sci.* **72**: 1783–1804.

Smith RK, Montgomery MT, Kilroy G, Tang S, Müller SK. 2015b. Tropical low formation during the Australian monsoon: The events of January 2013. *Aust. Meteorol. Oceanogr. J.* **65**: 318–341.

Tang S, Smith RK, Montgomery MT, Gu M. 2016. Numerical study of the spin-up of a tropical low over land during the Australian monsoon. *Q. J. R. Meteorol. Soc.* **142**: 2021–2032.

Vogl S, Smith RK. 2009. Limitations of a linear model for the hurricane boundary layer. *Q. J. R. Meteorol. Soc.* **135**: 839–850.

